

Submodularization for Binary Pairwise Energies

Lena Gorelick Yuri Boykov Olga Veksler
 Computer Science Department
 University of Western Ontario

Ismail Ben Ayed
 GE Healthcare

Andrew Delong
 Elect. & Comp. Engineering
 University of Toronto

Abstract

Many computer vision problems require optimization of binary non-submodular energies. We propose a general optimization framework based on local submodular approximations (LSA). Unlike standard LP relaxation methods that linearize the whole energy globally, our approach iteratively approximates the energies locally. On the other hand, unlike standard local optimization methods (e.g. gradient descent or projection techniques) we use non-linear submodular approximations and optimize them without leaving the domain of integer solutions. We discuss two specific LSA algorithms based on trust region and auxiliary function principles, LSA-TR and LSA-AUX. These methods obtain state-of-the-art results on a wide range of applications outperforming many standard techniques such as LBP, QPBO, and TRWS. While our paper is focused on pairwise energies, our ideas extend to higher-order problems. The code is available online¹.

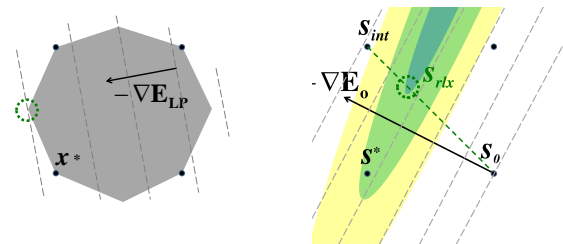
1. Introduction

We address a general class of binary pairwise non-submodular energies, which are widely used in applications like segmentation, stereo, inpainting, deconvolution, and many others. Without loss of generality, the corresponding binary energies can be transformed into the form²

$$E(S) = S^T U + S^T M S, \quad S \in \{0, 1\}^\Omega \quad (1)$$

where $S = \{s_p \mid p \in \Omega\}$ is a vector of binary indicator variables defined on pixels $p \in \Omega$, vector $U = \{u_p \in \mathcal{R} \mid p \in \Omega\}$ represents unary potentials, and symmetric matrix $M = \{m_{pq} \in \mathcal{R} \mid p, q \in \Omega\}$ represents pairwise potentials. Note that in many practical applications matrix M is sparse since elements $m_{pq} = 0$ for all non-interacting pairs of pixels. We seek solutions to the following integer quadratic optimization problem

$$\min_{S \in \{0, 1\}^\Omega} E(S). \quad (2)$$



(a) global linearization (b) local linearization

Figure 1. Standard linearization approaches for (1)-(2). Black dots are integer points and * corresponds to the global optimum of (2). Colors in (b) show iso-levels of the quadratic energy (1). This energy can be linearized by introducing additional variables and linear constraints, see a schematic polytope in (a) and [24]. Vector ∇E is the gradient of the global linearization of (1) in (a) and the gradient of the local linear approximation of (1) at point S_0 in (b).

When energy (1) is submodular, i.e. $m_{pq} \leq 0 \quad \forall(p, q)$, globally optimal solution for (2) can be found in a low-order polynomial time using graph cuts [3]. The general non-submodular case of problem (2) is NP hard.

1.1. Standard linearization methods

Integer quadratic programming problems is a well-known challenging optimization problem with extensive literature in the combinatorial optimization community, e.g. see [15, 9, 3]. It often appears in computer vision where it can be addressed with many methods including spectral and semi-definite programming relaxations, e.g. see [19, 12].

Methods for solving (2) based on LP relaxations, e.g. QPBO [21] and TRWS [13], are considered among the most powerful in computer vision [11]. They approach integer quadratic problem (2) by *global linearization* of the objective function at a cost of introducing a large number of additional variables and linear constraints. These methods attempt to optimize the relaxed LP or its dual. However, the integer solution can differ from the relaxed solution circled in Fig.1(a). This is a well-known *integrality gap* problem. Most heuristics for extracting an integer solution from the relaxed solution have no *a priori* quality guarantees.

Our work is more closely related to *local linearization*

¹<http://vision.csd.uwo.ca/code/>

²Note that such transformations are up to a constant.

techniques for approximating (2), e.g. parallel ICM, IPFP [16], and other similar methods [6]. Parallel ICM iteratively linearizes energy $E(S)$ around current solution S_0 using Taylor expansion and makes a step by computing an integer minimizer S_{int} of the corresponding linear approximation, see Fig.1(b). However, similarly to Newton’s methods, this approach often gets stuck in bad local minima by making too large steps regardless of the quality of the approximation. IPFP attempts to escape such minima by reducing the step size. It explores the continuous line between integer minimizer S_{int} and current solution S_0 and finds optimal relaxed solution S_{rlx} with respect to the original quadratic energy. Similarly to the global linearization methods, see Fig.1(a), such continuous solutions give no quality guarantees with respect to the original integer problem (2).

1.2. Overview of submodularization

Linearization has been a popular approximation approach to integer quadratic problem (1)-(2), but it often requires relaxation leading to the integrality gap problem. We propose a different approximation approach, which we refer to as *submodularization*. The main idea is to use submodular approximations of energy (1). We propose several approximation schemes that keep submodular terms in (1) and linearize non-submodular potentials in different ways leading to very different optimization algorithms. Standard *truncation* of non-submodular pairwise terms³ and some existing techniques for high-order energies [10, 17, 22, 2] can be seen as *submodularization* examples, as discussed later. Common properties of submodularization methods is that they compute globally optimal integer solutions of the approximation and do not need to leave the domain of discrete solutions avoiding integrality gaps. Submodularization can be seen as a generalization of local linearization methods since it uses more accurate higher-order approximations.

One way to linearize non-submodular terms in (1) is to compute their Taylor expansion around current solution S_0 . Taylor’s approach is similar to IPFP [16], but they linearize all terms including submodular ones. In contrast to IPFP, our overall approximation of $E(S)$ at S_0 is not linear; it belongs to a more general class of submodular functions. Such non-linear approximations are more accurate while still permitting efficient optimization in the integer domain.

We also propose a different mechanism for controlling the step size. Instead of exploring relaxed solutions on continuous interval $[S_0, S_{int}]$ in Fig.1b, we compute integer intermediate solutions S by minimizing local submodular approximation over $\{0, 1\}^\Omega$ under additional distance constraints $\|S - S_0\| < d$. Thus, our approach avoids integrality gap issues. For example, even linear approximation model in Fig.1b can produce solution S^* if Hamming distance constraint $\|S - S_0\| \leq 1$ is imposed. This local sub-

modularization approach to (1)-(2) fits a general *trust region framework* [8, 25, 19, 10] and we refer to it as LSA-TR.

Our paper also proposes a different local submodularization approach to (1)-(2) based on the general *auxiliary function* framework [14, 17, 2]⁴. Instead of Taylor expansion, non-submodular terms in $E(S)$ are approximated by linear upper bounds specific to current solution S_0 . Combining them with submodular terms in $E(S)$ gives a submodular upper-bound approximation, a.k.a. an *auxiliary function*, for $E(S)$ that can be globally minimized within integer solutions. This approach does not require to control the step sizes as the global minimizer of an auxiliary function is guaranteed to decrease the original energy $E(S)$. Throughout the paper we refer to this type of local submodular approximation approach as LSA-AUX.

Some auxiliary functions were previously proposed in the context of high-order energies [17, 2]. For example, [17] divided the energy into submodular and supermodular parts and replaced the latter with a certain permutation-based linear upper-bound. The corresponding auxiliary function allows polynomial-time solvers. However, experiments in [22] (Sec. 3.2) demonstrated limited accuracy of the permutation-based bounds [17] on high-order segmentation problems. Recently, Jensen inequality was used in [2] to derive linear upper bounds for several important classes of high-order terms that gave practically useful approximation results. Our LSA-AUX method is first to apply auxiliary function approach to arbitrary (non-submodular) pairwise energies. We discuss all possible linear upper bounds for pairwise terms and study several specific cases. One of them corresponds to the permutation bounds [17] and is denoted by LSA-AUX-P.

Recently both *trust region* [8, 25, 19] and *auxiliary function* [14] frameworks proved to work well for optimization of energies with high-order regional terms [10, 2]. They derive specific linear [10] or upper bound [2] approximations for non-linear cardinality potentials, KL and other distances between segment and target appearance models. To the best of our knowledge, we are the first to develop trust region and auxiliary function methods for integer quadratic optimization problems (1)-(2).

Our contributions can be summarized as follows:

- A general *submodularization* framework for solving integer quadratic optimization problems (1)-(2) based on *local submodular approximations* (LSA). Unlike global linearization methods, LSA constructs an approximation model without additional variables. Unlike local linearization methods, LSA uses a more accurate approximation functional.
- In contrast to the majority of standard approximation

³ Truncation is known to give low quality results, e.g. Fig.4, Tab.1.

⁴Auxiliary functions are also called *surrogate functions* or *upper-bounds*. The corresponding approximate optimization technique is also known as the *majorize-minimize* principle [14].

methods, LSA avoids integrality gap issue by working strictly within the domain of discrete solutions.

- State-of-the-art results on a wide range of applications. Our LSA algorithms outperform QPBO, LBP, IPFP, TRWS, its latest variant SRMP, and other standard techniques for (1)-(2).

2. Description of LSA Algorithms

In this section we discuss our framework in detail. Section 2.1 derives local submodular approximations and describes how to incorporate them in the trust region framework. Section 2.2 briefly reviews auxiliary function framework and shows how to derive local auxiliary bounds.

2.1. LSA-TR

Trust region methods are a class of iterative optimization algorithms. In each iteration, an approximate model of the optimization problem is constructed near the current solution S_0 . The model is only accurate within a small region around the current solution called “trust region”. The approximate model is then globally optimized within the trust region to obtain a candidate solution. This step is called *trust region sub-problem*. The size of the trust region is adjusted in each iteration based on the quality of the current approximation. For a detailed review of trust region framework see [25].

Below we provide details for our trust region approach to the binary pairwise energy optimization (see pseudo-code in Algorithm 1). The goal is to minimize $E(S)$ in (1). This energy can be decomposed into submodular and supermodular parts $E(S) = E^{sub}(S) + E^{sup}(S)$ such that

$$\begin{aligned} E^{sub}(S) &= S^T U + S^T M^- S \\ E^{sup}(S) &= S^T M^+ S \end{aligned}$$

where matrix M^- with negative elements $m_{pq}^- \leq 0$ represents the set of submodular pairwise potentials and matrix M^+ with positive elements $m_{pq}^+ \geq 0$ represents supermodular potentials. Given the current solution S_t energy $E(S)$ can be approximated by submodular function

$$E_t(S) = E^{sub}(S) + S^T U_t + const \quad (3)$$

where $U_t = 2M^+ S_t$. The last two terms in (3) are the first-order Taylor expansion of supermodular part $E^{sup}(S)$.

While the use of Taylor expansion may seem strange in the context of functions of integer variables, Figure 2(a,b) illustrates its geometric motivation. Consider individual pairwise supermodular potentials $f(x, y)$ in

$$E^{sup}(S) = \sum_{pq} m_{pq}^+ \cdot s_p s_q = \sum_{pq} f_{pq}(s_p, s_q).$$

Coincidentally, Taylor expansion of each relaxed supermodular potential $f(x, y) = \alpha \cdot xy$ produces a linear approximation (planes in b) that agrees with f at three out of four possible discrete configurations (points A,B,C,D).

The standard trust region sub-problem is to minimize approximation E_t within the region defined by step size d_t

$$S^* = \operatorname{argmin}_{\|S - S_t\| < d_t} E_t(S). \quad (4)$$

Hamming, L_2 , and other useful metrics $\|S - S_t\|$ can be represented by a sum of unary potentials [5]. However, optimization problem (4) is NP-hard even for unary metrics⁵. One can solve Lagrangian dual of (4) by iterative sequence of graph cuts as in [23], but the corresponding duality gap may be large and the optimum for (4) is not guaranteed.

Instead of (4) we use a simpler formulation of the trust region subproblem proposed in [10]. It is based on unconstrained optimization of submodular Lagrangian

$$L_t(S) = E_t(S) + \lambda_t \cdot \|S - S_t\| \quad (5)$$

where parameter λ_t controls the trust region size indirectly. Each iteration of LSA-TR solves (5) for some fixed λ_t and adaptively changes λ_t for the next iteration (Alg.1 line 10), as motivated by empirical inverse proportionality relation between λ_t and d_t discussed in [10].

Once a candidate solution S^* is obtained, the quality of the approximation is measured using the ratio between the actual and predicted reduction in energy. Based on this ratio, the solution is updated in line 8 and the step size (or λ) is adjusted in line 10. It is common to set the parameter τ_1 in line 8 to zero, meaning that any candidate solution that decreases the actual energy gets accepted. The parameter τ_2 in line 10 is usually set to 0.25 [25]. Reduction ratio above this value corresponds to good approximation model allowing increase in the trust region size.

Algorithm 1: GENERAL TRUST REGION APPROACH

- 1 **Initialize** $t = 0, S_0, \lambda_0$
 - 2 **Repeat**
 - 3 **//Solve Trust Region Sub-Problem**
 - 4 $S^* \leftarrow \operatorname{argmin}_{S \in \{0,1\}^\Omega} L_t(S)$ // as defined in (5)
 - 5 $P = E_t(S_t) - E_t(S^*)$ //predicted reduction in energy
 - 6 $R = E(S_t) - E(S^*)$ //actual reduction in energy
 - 7 **//Update current solution**
 - 8 $S_{t+1} \leftarrow \begin{cases} S^* & \text{if } R/P > \tau_1 \\ S_t & \text{otherwise} \end{cases}$
 - 9 **//Adjust the trust region**
 - 10 $\lambda_{t+1} \leftarrow \begin{cases} \lambda_t/\alpha & \text{if } R/P > \tau_2 \\ \lambda_t \cdot \alpha & \text{otherwise} \end{cases}$
 - 11 **Until Convergence**
-

⁵By a reduction to the *balanced cut* problem.

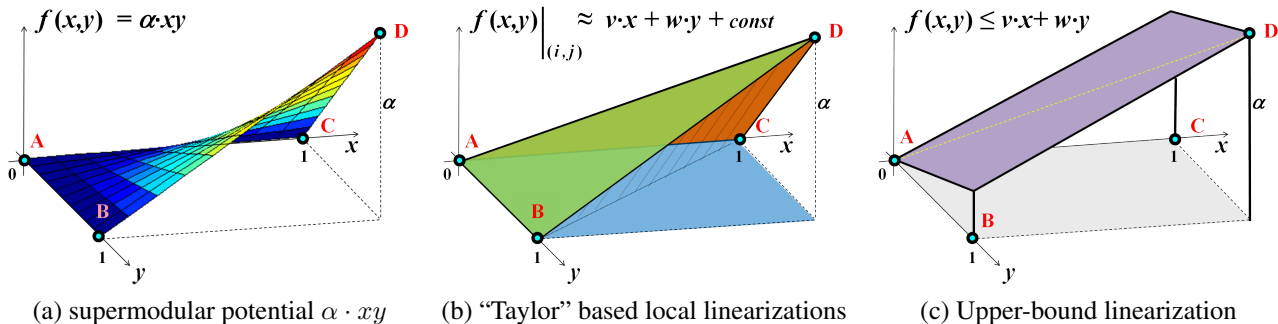


Figure 2. Local linearization of supermodular pairwise potential $f(x, y) = \alpha \cdot xy$ for $\alpha > 0$. This potential defines four costs $f(0, 0) = f(0, 1) = f(1, 0) = 0$ and $f(1, 1) = \alpha$ at four distinct configurations of binary variables $x, y \in \{0, 1\}$. These costs can be plotted as four 3D points A, B, C, D in (a-c). We need to approximate supermodular potential f with a linear function $v \cdot x + w \cdot y + const$ (plane or unary potentials). **LSA-TR**: one way to derive a local linear approximation is to take Taylor expansion of $f(x, y) = \alpha \cdot xy$ over relaxed variables $x, y \in [0, 1]$, see the continuous plot in (a). At first, this idea may sound strange since there are infinitely many other continuous functions that agree with A, B, C, D but have completely different derivatives, e.g. $g(x, y) = \alpha \cdot x^2 \sqrt{y}$. However, Taylor expansions of **bilinear** function $f(x, y) = \alpha \cdot xy$ can be motivated geometrically. As shown in (b), Taylor-based local linear approximation of f at any fixed integer configuration (i, j) (e.g. blue plane at A , green at B , orange at C , and striped at D) coincides with discrete pairwise potential f not only at point (i, j) but also with two other closest integer configurations. Overall, each of those planes passes exactly through three out of four points A, B, C, D . **LSA-AUX**: another approach to justify a local linear approximation for non-submodular pairwise potential f could be based on upper bounds passing through a current configuration. For example, the green or orange planes in (b) are the tightest linear upper bounds at configurations $(0, 1)$ and $(1, 0)$, correspondingly. When current configuration is either $(0, 0)$ or $(1, 1)$ then one can choose either orange or green plane in (b), or anything in-between, e.g. the purple plane passing through A and D in (c).

2.2. LSA-AUX

Bound optimization techniques are a class of iterative optimization algorithms constructing and optimizing upper bounds, a.k.a. *auxiliary functions*, for energy E . It is assumed that those bounds are easier to optimize than the original energy E . Given a current solution S_t , the function $A_t(S)$ is an auxiliary function of E if it satisfies the following conditions:

$$E(S) \leq A_t(S) \tag{6a}$$

$$E(S_t) = A_t(S_t) \tag{6b}$$

To approximate minimization of E , one can iteratively minimize a sequence of auxiliary functions:

$$S_{t+1} = \arg \min_S A_t(S), \quad t = 1, 2, \dots \tag{7}$$

Using (6a), (6b), and (7), it is straightforward to prove that the solutions in (7) correspond to a sequence of decreasing energy values $E(S_t)$. Namely,

$$E(S_{t+1}) \leq A_t(S_{t+1}) \leq A_t(S_t) = E(S_t).$$

The main challenge in bound optimization approach is designing an appropriate auxiliary function satisfying conditions (6a) and (6b). However, in case of integer quadratic optimization problem (1)-(2), it is fairly straightforward to design an upper bound for non-submodular energy $E(S) = E^{sub}(S) + E^{sup}(S)$. As in Sec.2.1, we do not need to approximate the submodular part E^{sub} and we can easily find a linear upper bound for E^{sup} as follows.

Similarly to Sec.2.1, consider supermodular pairwise potentials $f(x, y) = \alpha \cdot xy$ for individual pairs of neighboring pixels according to

$$E^{sup}(S) = \sum_{pq} m_{pq}^+ \cdot s_p s_q = \sum_{pq} f_{pq}(s_p, s_q) \tag{8}$$

where each f_{pq} is defined by scalar $\alpha = m_{pq}^+ > 0$. As shown in Figure 2(b,c), each pairwise potential f can be bound above by linear function $u(x, y)$

$$f(x, y) \leq u(x, y) := v \cdot x + w \cdot y$$

for some positive scalars v and w . Assuming current solution $(x, y) = (x^t, y^t)$, the table below specifies linear upper bounds (planes) for four possible discrete configurations

(x^t, y^t)	upper bound $u(x, y)$	plane in Fig.2(b,c)
(0,0)	$\frac{\alpha}{2}x + \frac{\alpha}{2}y$	purple
(0,1)	αx	green
(1,0)	αy	orange
(1,1)	$\frac{\alpha}{2}x + \frac{\alpha}{2}y$	purple

As clear from Fig.2(b,c), there are many other possible linear upper bounds for pairwise terms f . Interestingly, the “permutation” approach to high-order supermodular terms in [17] reduces to linear upper bounds for $f(x, y)$ where each configuration $(0,0)$ or $(1,1)$ selects either orange or green plane randomly (depending on a permutation). Our tests showed inferior performance of such bounds for pairwise energies. The upper bounds using purple planes for $(0,0)$ and $(1,1)$, as in the table, work better in practice.

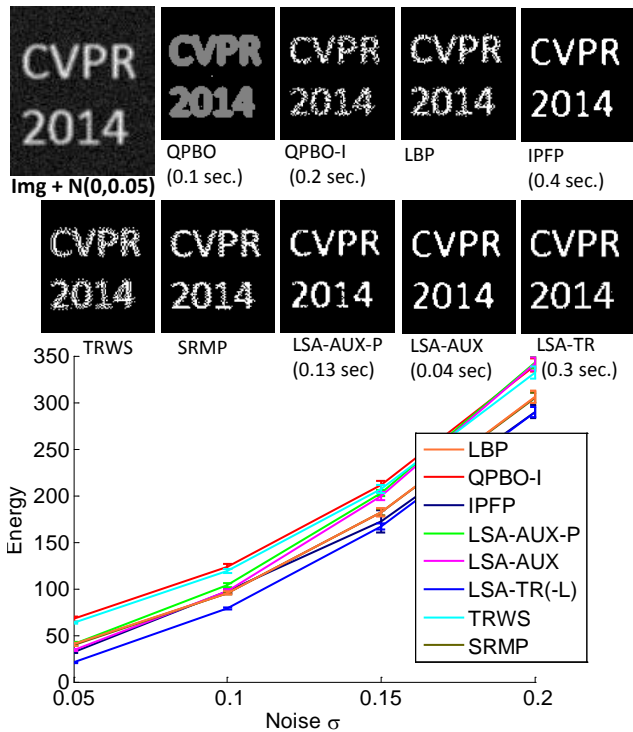


Figure 3. Binary deconvolution of an image created with a uniform 3×3 filter and additive Gaussian noise ($\sigma \in \{0.05, 0.1, 0.15, 0.2\}$). No length regularization was used. We report mean energy (+/-2std.) and time as a function of noise level σ . TRWS, SRMP and LBP are run for 5000 iterations.

Summing upper bounds for all pairwise potentials f_{pq} in (8) using linear terms in this table gives an overall linear upper bound for supermodular part of energy (1)

$$E^{sup}(S) \leq S^T U_t \quad (9)$$

where vector $U_t = \{u_p^t | p \in \Omega\}$ consists of elements

$$u_p^t = \sum_q \frac{m_{pq}^+}{2} (1 + s_p^t - 2s_p^t s_q^t)$$

and $S_t = \{s_p^t | p \in \Omega\}$ is the current solution configuration for all pixels. Defining our auxiliary function as

$$A_t(S) := S^T U_t + E^{sub}(S) \quad (10)$$

and using inequality (9) we satisfy condition (6a)

$$E(S) = E^{sup}(S) + E^{sub}(S) \leq A_t(S).$$

Since $S_t^T U_t = E^{sup}(S_t)$ then our auxiliary function (10) also satisfies condition (6b)

$$E(S_t) = E^{sup}(S_t) + E^{sub}(S_t) = A_t(S_t).$$

Function $A_t(S)$ is submodular. Thus, we can globally optimize it in each iterations guaranteeing energy decrease.

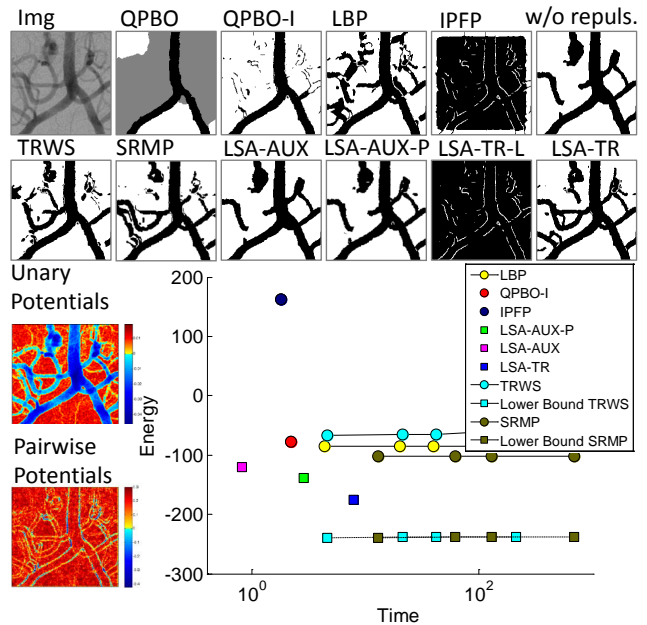


Figure 4. Segmentation with repulsion and attraction. We used $\mu_{fg}=0.4$, $\mu_{bg}=0.6$, $\sigma=0.2$ for appearance, $\lambda_{reg}=100$ and $c=0.06$. Repulsion potentials are shown in blue and attraction - in red.

3. Applications

Below we apply our method in several applications such as binary deconvolution, segmentation with repulsion, curvature regularization and inpainting. We report results for both LSA-TR and LSA-AUX frameworks and compare to existing state of the art methods such as QPBO [21], LBP [20], IPFP [16], TRWS and SRMP [13] in terms of energy and running time⁶. For the sake of completeness, and to demonstrate the advantage of non-linear submodular approximations over linear approximations, we also compare to a version of LSA-TR where both submodular and supermodular terms are linearized, denoted by LSA-TR-L. In the following experiments, all local approximation methods, e.g. IPFP, LSA-AUX, LSA-AUX-P, LSA-TR, LSA-TR-L are initialized with the entire domain assigned to the foreground. All global linearization methods, e.g. TRWS, SRMP and LBP, are run for 50, 100, 1000 and 5000 iterations. For QPBO results, unlabeled pixels are shown in gray color. Running time is shown in log-scale for clarity.

3.1. Binary Deconvolution

Figures 3 (top-left) shows a binary image after convolution with a uniform 3×3 and adding Gaussian noise ($\sigma = 0.05$). The goal of binary deconvolution is to recover

⁶We used <http://pub.ist.ac.at/~vnk/software.html> code for SRMP and www.robots.ox.ac.uk/~ojw code for QPBO, TRWS, and LBP. The corresponding version of LBP is sequential without damping.

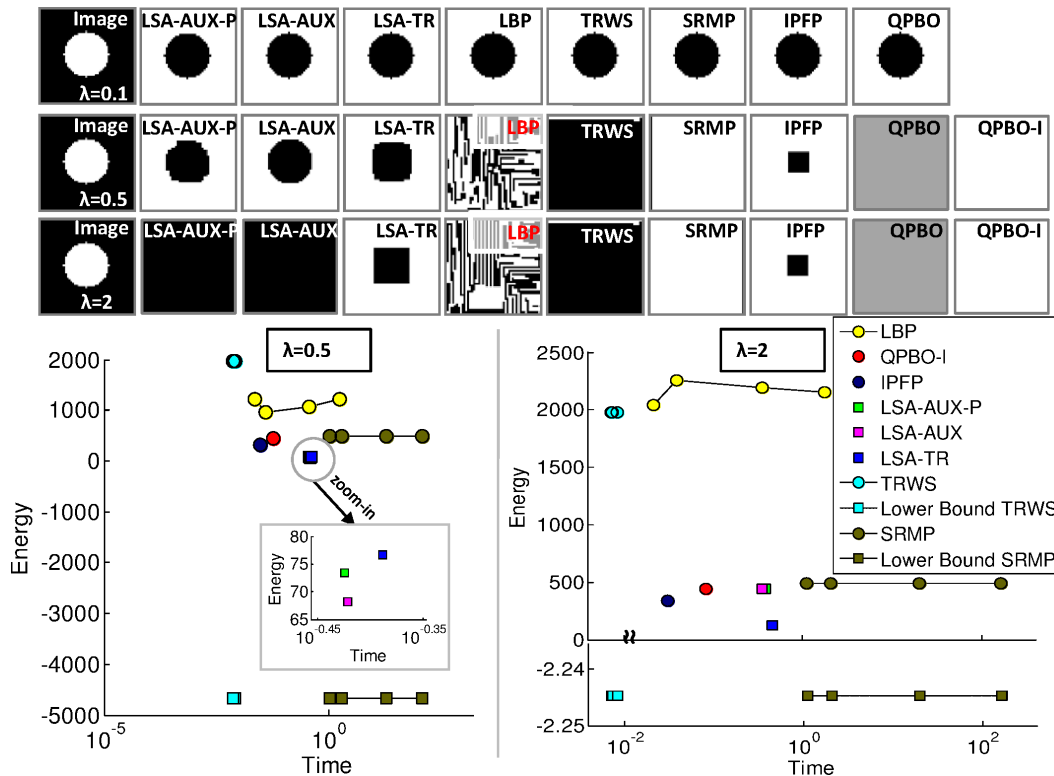


Figure 5. Curvature regularizer [7] is more difficult to optimize when regularizer weight is high. We show segmentation results for $\lambda_{curv} = 0.1$ (top row), $\lambda_{curv} = 0.5$ (middle row), $\lambda_{curv} = 2$ (bottom row) as well as energy plots. We used $\mu_{fg} = 1$, $\mu_{bg} = 0$, $\lambda_{app} = 1$.

the original binary image and the energy is defined as

$$E(S) = \sum_{p \in \Omega} (I_p - \frac{1}{9} \sum_{q \in \mathcal{N}_p} s_q)^2 \quad (11)$$

Here \mathcal{N}_p denotes the 3×3 neighborhood window around pixel p and all pairwise interactions are supermodular. We did not use length regularization, since it would make the energy easier to optimize. Fig. 3 demonstrates the performance of our approach (LSA-TR/LSA-AUX) and compares to standard optimization methods such as QPBO, LBP, IPFP, TRWS and SRMP. In this case LSA-TR-L and LSA-TR are identical since energy (11) has no submodular pairwise terms. The bottom of Fig. 3 shows the mean energy as a function of noise level σ . For each experiment the results are averaged over ten instances of random noise. The mean time is reported for the experiments with $\sigma = 0.05$.

3.2. Segmentation with Repulsion

In this section we consider segmentation with attraction and repulsion pairwise potentials. Adding repulsion is similar to correlation clustering [1], where data points either attract or repulse each other. Using negative repulsion in segmentation can avoid the bias of submodular length regularizer to *short-cutting*, whereby elongated structures are

shortened to avoid high length penalty. Figure 4 (top-left) shows an example of an angiogram image with elongated structures. We use 16-neighborhood system and the pairwise potentials are defined as follows:

$$\omega(p, q) = \frac{-\Delta(p, q) + c}{\text{dist}(p, q)}.$$

Here $\text{dist}(p, q)$ denotes the distance between image pixels p and q and $\Delta(p, q)$ is the difference in their respective intensities (see pairwise potentials in Fig. 4, bottom-left). The constant c is used to make neighboring pixels with similar intensities attract and repulse otherwise. Being supermodular, repulsions potentials make the segmentation energy more difficult to optimize, but are capable to extract thin elongated structures. To demonstrate the usefulness of “repulsion” potentials we also show segmentation results with graph-cut a la Boykov-Jolly [4] where negative pairwise potentials were removed/truncated (top-right).

3.3. Curvature

Below we apply our optimization method to curvature regularization. We focus on the curvature model proposed in [7]. The model is defined in terms of 4-neighborhood system and accounts for 90 degrees angles. In combination with appearance terms, the model yields discrete bi-

nary energy that has both submodular and non-submodular pairwise potentials. Originally, the authors of [7] proposed using QPBO for optimization of the curvature regularizer. We show that our method significantly outperforms QPBO and other state-of-the-art optimization techniques, especially with large regularizer weights.

First we deliberately choose a toy example (white circle on a black background, see Fig. 5) where we know what an optimal solution should look like. When using 4-neighborhood system, as the weight of the curvature regularizer increases, the solution should minimize the number of 90 degrees angles (corners) while maximizing the appearance terms. Therefore, when the weight of curvature regularizer is high, the solution should look more like a square than a circle. Consider the segmentation results in Fig. 5. With low curvature weight, i.e., $\lambda_{curv} = 0.1$, all compared methods perform equally well (see Fig. 5 top row). In this case appearance data terms are strong compared to the non-submodular pairwise terms. However, when we increase the curvature weight and set $\lambda_{curv} = 0.5$ or 2 there is a significant difference between the optimization methods both in terms of the energy and the resulting solutions (see Fig. 5 middle and bottom).

Next, we selected an angiogram image example from [7] and evaluate the performance⁷ of the optimization methods with two values of regularizer weight $\lambda_{curv} = 19$ and $\lambda_{curv} = 21$ (see Fig. 7). Although the weight λ did not change significantly, the quality of the segmentation deteriorated for all global linearization methods, namely QPBO, TRWS, LBP. The proposed methods LSA-TR and LSA-AUX seem to be robust with respect to the weight of the supermodular part of the energy.

3.4. Chinese Characters Inpainting

Below we consider the task of in-painting in binary images of Chinese characters, *dtf-chinesechar* [11]. We used a set of pre-trained unary and pairwise potentials provided by the authors with the dataset. While each pixel variable has only two possible labels, the topology of the resulting graph and the non-submodularity of its pairwise potentials makes this problem challenging. Figure 6 shows two examples of inpainting. Table 1 reports the performance of our LSA-TR and LSA-AUX methods on this problem and compares to other standard optimization methods reported in [11], as well as, to *truncation* of non-submodular terms. LSA-TR is ranked second, but runs three orders of magnitudes faster.

4. Conclusions and Future Work

There are additional applications (beyond the scope of this paper) that can benefit from efficient optimization of

⁷For QPBO, we only run QPBO-I and do not use other post-processing heuristics as suggested in [7], since the number of unlabeled pixel might be significant when the regularization is strong.



Figure 6. Examples of Chinese characters inpainting.

Alg. Name	Mean Runtime	Mean Energy	#best /100	Rank
MCBC	2053.89 sec	-49550.1	85	1
BPS (LBP)*	72.85 sec	-49537.08	18	3
ILP	3580.93 sec	-49536.59	8	6
QPBO	0.16 sec	-49501.95	0	8
SA	NaN sec	-49533.08	13	4
TRWS	0.13 sec	-49496.84	2	7
TRWS-LF	2106.94 sec	-49519.44	11	5
Truncation	0.06 sec	-16089.2	0	8
LSA-AUX	0.30 sec	-49515.95	0	8
LSA-AUX-P	0.16 sec	-49516.63	0	8
LSA-TR	0.21 sec	-49547.61	35	2

Table 1. Chinese characters in-painting database [11]. We tested three methods (at the bottom) and compared with other techniques (above) reported in [11]. * - To the best of our knowledge, BPS in [11] is the basic sequential version of loopy belief-propagation without damping that we simply call LBP in this paper.

binary non-submodular pairwise energies. For instance, our experiments show that our approach can improve non-submodular α -expansion and fusion moves for multilabel energies. Moreover, while our paper focuses on pairwise interactions, our approach naturally extends to high-order potentials that appear in computer vision problems such as curvature regularization, convexity shape prior, visibility and silhouette consistency in multi-view reconstruction. In the companion paper [18] we apply our method for optimization of a new highly accurate curvature regularization model. The model yields energy with triple clique interactions and our method achieves state-of-the-art performance.

Acknowledgments

We greatly thank V. Kolmogorov and our anonymous reviewers for their thorough feedback. We also thank NSERC and NIH for their grants supporting this project.

References

- [1] N. Bansal, A. Blum, and S. Chawla. Correlation clustering. In *Machine Learning*, volume 56, pages 89–113, 2004. 6
- [2] I. Ben Ayed, L. Gorelick, and Y. Boykov. Auxiliary cuts for general classes of higher order functionals. In *IEEE conference on Computer Vision and Pattern Recognition (CVPR)*, pages 1304–1311, Portland, Oregon, June 2013. 2

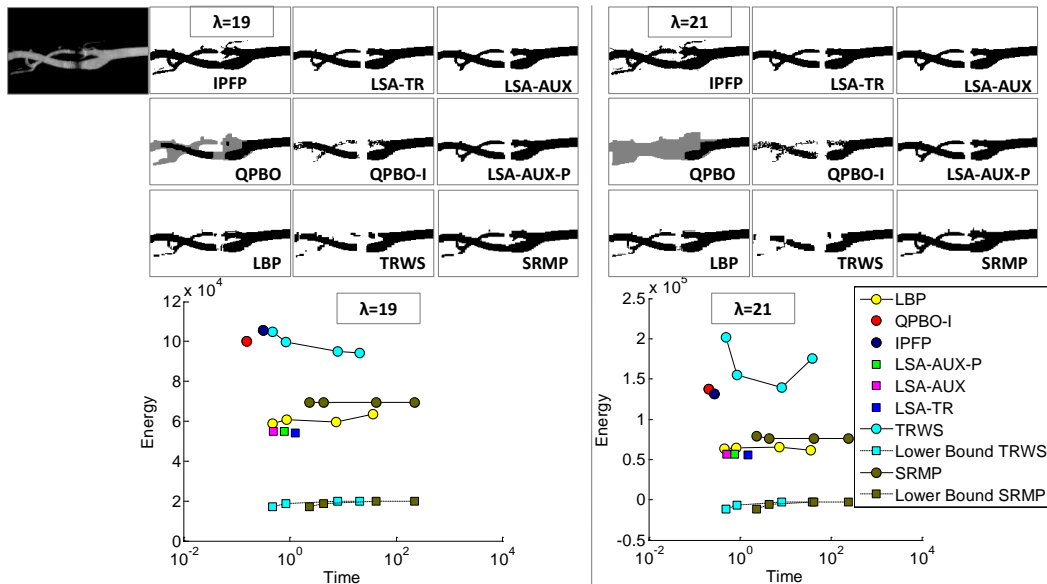


Figure 7. Curvature regularizer [7]: we show segmentation results and energy plots for $\lambda_{curv}=19$ (left), $\lambda_{curv}=21$ (right).

[3] E. Boros and P. L. Hammer. Pseudo-boolean optimization. *Discrete Applied Mathematics*, 123:2002, 2001. 1

[4] Y. Boykov and M.-P. Jolly. Interactive graph cuts for optimal boundary and region segmentation of objects in n-d images. In *IEEE International Conference on Computer Vision (ICCV)*, number 105-112, 2001. 6

[5] Y. Boykov, V. Kolmogorov, D. Cremers, and A. Delong. An integral solution to surface evolution PDEs via Geo-Cuts. In *European Conf. on Comp. Vision (ECCV)*. 3

[6] W. Brendel and S. Todorovic. Segmentation as maximum-weight independent set. In *Neural Information Processing Systems (NIPS)*, pages 307–315, 2010. 2

[7] N. El-Zehiry and L. Grady. Fast global optimization of curvature. In *IEEE conference on Computer Vision and Pattern Recognition (CVPR)*, number 3257-3264, 2010. 6, 7, 8

[8] R. Fletcher. *Practical Meth. of Opt.* Wiley & Sons, 1987. 2

[9] M. Goemans and D. Williamson. Improved approximation algorithms for maximum cut and satisfiability problem using semidefinite problem. *ACM*, 42(6):1115–1145, 1995. 1

[10] L. Gorelick, F. R. Schmidt, and Y. Boykov. Fast trust region for segmentation. In *IEEE conference on Computer Vision and Pattern Recognition (CVPR)*, pages 1714–1721, Portland, Oregon, June 2013. 2, 3

[11] J. H. Kappes, B. Andres, F. A. Hamprecht, C. Schnorr, S. Nowozin, D. Batra, S. Kim, B. X. Kausler, J. Lellmann, N. Komodakis, and C. Rother. A comparative study of modern inference techniques for discrete energy minimization problem. In *IEEE conference on Computer Vision and Pattern Recognition (CVPR)*, pages 1328–1335, 2013. 1, 7

[12] J. Keuchel, C. Schnörr, C. Schellewald, and D. Cremers. Binary partitioning, perceptual grouping, and restoration with semidefinite programming. 25(11):1364–1379, 2003. 1

[13] V. Kolmogorov and T. Schoenemann. Generalized seq. tree-reweighted message passing. *arXiv:1205.6352*, 2012. 1, 5

[14] K. Lange, D. R. Hunter, and I. Yang. Optimization transfer using surrogate objective functions. *Journal of Computational and Graphical Statistics*, 9(1):1–20, 2000. 2

[15] R. Lazimy. Mixed integer quadratic programming. *Mathematical Programming*, 22:332–349, 1982. 1

[16] M. Leordeanu, M. Hebert, and R. Sukthankar. An integer projected fixed point method for graph matching and map inference. In *Neural Information Processing Systems (NIPS)*, pages 1114–1122, 2009. 2, 5

[17] M. Narasimhan and J. A. Bilmes. A submodular-supermodular procedure with applications to discriminative structure learning. In *UAI*, pages 404–412, 2005. 2, 4

[18] C. Nieuwenhuis, E. Toeppe, L. Gorelick, O. Veksler, and Y. Boykov. Efficient Squared Curvature. In *IEEE conf. on Comp. Vision and Pattern Recognition (CVPR)*, 2014. 7

[19] C. Olsson, A. Eriksson, and F. Kahl. Improved spectral relaxation methods for binary quadratic optimization problems. *Comp. Vis. & Image Underst.*, 112(1):3–13, 2008. 1, 2

[20] J. Pearl. Reverend bayes on inference engines: A distributed hierarchical approach. In *National Conference on Artificial Intelligence*, pages 133–136, 1982. 5

[21] C. Rother, V. Kolmogorov, V. Lempitsky, and M. Szummer. Optimizing binary MRFs via extended roof duality. In *IEEE conference on Computer Vision and Pattern Recognition (CVPR)*, pages 1–8, 2007. 1, 5

[22] C. Rother, V. Kolmogorov, T. Minka, and A. Blake. Cosegmentation of Image Pairs by Histogram Matching - Incorporating a Global Constraint into MRFs. In *Computer Vision and Pattern Recognition (CVPR)*, pages 993 – 1000, 2006. 2

[23] J. Ulen, P. Strandmark, and F. Kahl. An efficient optimization framework for multi-region segmentation based on Lagrangian duality. *IEEE Transactions on Medical Imaging*, 32(2):178–188, 2013. 3

[24] M. J. Wainwright and M. I. Jordan. Graphical models, exponential families, and variational inference. *Foundations and Trends in Machine Learning*, 1(1-2):1–305, 2008. 1

[25] Y. Yuan. A review of trust region algorithms for optimization. In *Proceedings of the Fourth International Congress on Industrial & Applied Mathematics (ICIAM)*, 1999. 2, 3